


Galaxy Alignments with Surrounding Structure in the Sloan Digital Sky Survey

DHVANIL D. DESAI ^{1,2} AND BARBARA S. RYDEN ^{1,3}¹*Department of Astronomy, The Ohio State University, 140 W. 18th Ave., Columbus, OH 43210 USA*²*Institute for Astronomy, University of Hawaii, 2680 Woodlawn Drive, Honolulu, HI 96822 USA*³*Center for Cosmology & Astroparticle Physics, The Ohio State University, 191 W. Woodruff Ave., Columbus, OH 43210 USA*

ABSTRACT

Using data from the Sloan Digital Sky Survey (SDSS) Legacy Survey, we study the alignment of luminous galaxies with spectroscopic data with the surrounding larger-scale structure as defined by galaxies with only photometric data. We find that galaxies from the red sequence have a statistically significant tendency for their apparent long axes to align parallel to the projected surrounding structure. Red galaxies more luminous than the median of our sample ($M_r < -21.78$) have a mean alignment angle $\langle \Phi \rangle < 45^\circ$, indicating preferred parallel alignment, at a significance level $> 4.5\sigma$ on projected scales $0.1 \text{ Mpc} < r_p \leq 7.5 \text{ Mpc}$. Fainter red galaxies have $\langle \Phi \rangle < 45^\circ$ at a significance level $> 4.3\sigma$ at scales $1 \text{ Mpc} < r_p < 3 \text{ Mpc}$. At a projected scale $r_p = 3.0 \text{ Mpc}$, the mean alignment angle decreases steadily with increasing luminosity for red galaxies with $M_r \lesssim -22.5$, reaching $\langle \Phi \rangle = 40.49^\circ \pm 0.56^\circ$ for the most luminous one percent ($M_r \sim -23.57$). Galaxies from the blue sequence show no statistically significant tendency for their axes to align with larger-scale structure, regardless of galaxy luminosity. Galaxies in higher-density regions do not show a statistically significant difference in mean alignment angle from galaxies in lower-density regions; this holds true for the faint blue, luminous blue, faint red, and luminous red subsets.

Keywords: clustering — cosmic web — galaxy properties — large-scale structure of the universe

1. INTRODUCTION AND BACKGROUND

The study of the intrinsic alignment of galaxies with larger scale structure has a long history (Brown 1939; Wyatt & Brown 1955; Reaves 1958; Brown 1964). Statistical analysis of these intrinsic alignments can shed light on how the large-scale structure of the universe affects the formation and evolution of galaxies. Luminous late-type galaxies, for example, have rotationally supported disks. Tidal torque theory (Hoyle 1951; Peebles 1969) explains how disk galaxies are spun up through the interaction of a protogalaxy’s quadrupole moment with the tidal field of the surrounding matter distribution. Thus, it is reasonable to assume some sort of alignment between the disk’s angular momentum vector and the surrounding large-scale structure. In addition, the outer regions of early-type galaxies will also be shaped by the tidal gravitational field of surrounding matter (Catelan et al. 2001; Reischke & Schäfer 2019). The predictions

of tidal torque theory can be extended into the nonlinear regime by analytic methods (Catelan et al. 2001; Bridle & King 2007; Blazek et al. 2015; Ebrahimi & Abolhasani 2022).

The use of numerical simulations to study the evolution of intrinsic alignments allows the introduction of non-gravitational effects. Generally, simulations show that more massive and more luminous galaxies show stronger alignment signals (Hilbert et al. 2017; Ganeshiah Veena et al. 2019; Tenneti et al. 2021). The evolution of intrinsic alignment in numerical simulations is found to depend on many factors (Bhowmick et al. 2020). In general, high-mass galaxies have an alignment signal that increases from $z \sim 1$ to $z \sim 0$ (Zjupa et al. 2020; Samuroff et al. 2020); however, low-mass galaxies tend to have an alignment that decreases with time (Codis et al. 2018). Numerical simulations also permit a full three-dimensional view of how galaxies are oriented with respect to different structures in the cosmic web. For instance, Codis et al. (2018) find that the spin axis of low-mass galaxies aligns with filaments in the cosmic web, while the spin axis of higher-mass galaxies aligns perpendicular to filaments.

Observational studies of intrinsic alignment generally require using data from large surveys, given the weakness of the alignment signal. Within the Local Group, for instance, alignments are difficult to detect with high statistical significance, even with ultra-faint dwarfs added to the sample (Sanders & Evans 2017). However, a deeper study of $N \sim 6000$ systems similar to the Local Group, dominated by two luminous galaxies, reveals that satellites between the two spirals tend to have their projected long axis perpendicular to the line connecting the bright primary galaxies, while outer satellites tend to be radially aligned (Wang et al. 2019). In larger groups containing a single bright galaxy, satellite galaxies tend to align with the apparent long axis of the brightest group galaxy, with red satellites showing a stronger alignment signal than blue satellites (Georgiou et al. 2019a). In addition to alignments between satellite galaxies and the group or cluster in which they are found, alignments are also seen between the satellite distribution and filaments in the cosmic web (Wang et al. 2020). Several studies, reviewed by Joachimi et al. (2015), indicate that disk galaxies tend to align their spin perpendicular to the direction of filaments in the large-scale structure. However, a more recent MaNGA survey (Kraljic et al. 2021) indicates that while S0 galaxies tend to have a spin axis perpendicular to the nearest filament, spirals of later type tend to have their spin axis parallel to the nearest filament. In addition, the alignment signal for late-type galaxies is weaker than the signal for early-type galaxies, which tend to align their apparent major axes parallel to the direction of filaments (Joachimi et al. 2015; Chen et al. 2019).

Observational studies emphasize that red, early-type galaxies tend to have a stronger alignment than blue, late-type galaxies (Joachimi et al. 2015; Johnston et al. 2019). Tonegawa & Okumura (2022) find that red galaxies show detectable alignment at redshifts as high as $z \sim 1.3$, at the 2.5σ level. Among the population of red galaxies, the most luminous galaxies show the strongest alignment signal (Fortuna et al. 2021; Rodriguez et al. 2022).

The study of intrinsic alignments, in addition to giving insight into the formation and evolution of large-scale structure, is essential for interpreting the results of weak gravitational lensing measurements (Gunn 1967; Okumura & Jing 2009). Weak lensing by the intervening mass distribution produces a shear distortion in a distant galaxy’s image. Although intrinsic alignment is sometimes described as a “contaminant” of the image alignment caused by weak gravitational lensing, the same tidal shear fields that create weak lensing distortions can also physically distort the outer regions of a

galaxy (Pedersen et al. 2020; Ghosh et al. 2021). By studying galaxies at low redshift ($z \lesssim 0.1$), where the weak lensing effect is negligible compared to intrinsic alignments, we can quantify the intrinsic alignment signal on its own. Given the known dependence of intrinsic alignment on galaxy color and luminosity, we will be careful to distinguish between red, early-type galaxies and blue, late-type galaxies in our study of galaxy alignment with surrounding structure, and will pay particular attention to the dependence of the alignment on the galaxy’s luminosity.

2. DATA AND DEFINITIONS

Our study used galaxy data from the Legacy Survey of the Sloan Digital Sky Survey (SDSS) (York et al. 2000; Gunn et al. 2006). Data were downloaded from Data Release 16 of the SDSS (Ahumada et al. 2020). The SDSS Legacy imaging survey covered $14,555 \text{ deg}^2$, recording imaging data for ~ 50 million galaxies; the SDSS Legacy spectroscopic survey provided spectroscopic data for ~ 1.5 million of those galaxies (Eisenstein et al. 2011). The SDSS database has proved highly valuable for studies of the alignment of galaxy images with larger scale structure (Lee & Pen 2007; Hirata et al. 2007; Wang et al. 2008; Paz et al. 2008; Okumura et al. 2009; Jones et al. 2010; Zhang et al. 2013, 2015; Hirv et al. 2017; Wang et al. 2018, 2020; Zhang et al. 2020). The footprint of the SDSS Legacy survey is sufficiently large to allow the detection of alignments on scales of $\sim 10 \text{ Mpc}$ or larger (Smargon et al. 2012; Chen et al. 2019). In this paper, we use SDSS Legacy data to study the alignment of “target galaxies,” drawn from the spectroscopic survey and thus having accurate spectroscopic redshifts, with the larger scale structure defined by “surrounding galaxies,” drawn from the imaging survey and thus having only imprecise photometric redshifts.

The SDSS imaging survey used five broadband filters u , g , r , i , and z (Fukugita et al. 1996; Doi et al. 2010). Photometric parameters in the r band (effective wavelength $\lambda_r = 6261 \text{ \AA}$) were used to determine the location, axis ratio, and orientation of the galaxies in our sample. Galaxy axis ratios and orientation can be wavelength-dependent (Georgiou et al. 2019b). Since galaxies tend to be bluer with increasing radius, choosing the r band, rather than a shorter-wavelength band, de-emphasizes the contributions of the outer regions of target galaxies. The $u - r$ color index was used to define the color of galaxies. The u band, with effective wavelength $\lambda_u = 3557 \text{ \AA}$, is sensitive to the presence of hot stars; thus the $u - r$ color index is a good diagnostic of the presence of recent star formation. From the SDSS table `PhotoObj`, following the suggestion of Scran-

ton et al. (2005), `cModelMag_r` was used for the absolute r band magnitude and `modelMag_r` and `modelMag_u` were used for the $u - r$ color index.¹

The SDSS spectroscopic survey, from which we drew our target galaxies, is complete to a limiting r band magnitude $r = 17.77$ (Strauss et al. 2002). We selected target galaxies with spectroscopic redshifts in the range $0.02 < z < 0.25$. The lower redshift limit eliminates galaxies whose peculiar motion contributes significantly to the redshift. The higher redshift limit mostly excludes galaxies that form the Luminous Red Galaxy (LRG) sample (Eisenstein et al. 2001). The excluded higher redshift galaxies have a median absolute magnitude $M_r = -22.69$ and median color $u - r = 3.08$. Adding these LRGs to our sample would not greatly contribute to our goal of identifying how alignment properties differ between the red sequence and the blue sequence of galaxies, and by eliminating them from our sample, we reduce possible effects of evolution ($z = 0.25$ corresponds to a lookback time $t \approx 3.0$ Gyr) and of weak lensing shear.

We compute distance modulus as a function of spectroscopic redshift $\mu(z)$ using the Python package `astropy.cosmology` (Astropy Collaboration et al. 2013, 2018), assuming a flat Λ CDM cosmology with parameters from the *Planck* 2018 results (Planck Collaboration et al. 2020). In particular, this assumes $H_0 = 67.4 \text{ km s}^{-1} \text{ Mpc}^{-1}$ and $\Omega_{m,0} = 0.315$. We corrected the u and r band magnitudes for Galactic extinction exactly as done by the SDSS pipeline; this correction uses the dust map of Schlegel et al. (1998), and assumes a 7000 K source and a ratio of total to selective extinction $R_V = 3.1$ (Schlafly & Finkbeiner 2011). For each extragalactic source, the correction yields an estimated Galactic extinction $A_{u,Gal}$ and $A_{r,Gal}$. The K -correction for each source (Hogg et al. 2002) was done using the code of Blanton & Roweis (2007). The absolute r band magnitude is then

$$M_r = r - \mu(z) - A_{r,Gal} - K_r(z) \quad (1)$$

and the corrected $u - r$ color is

$$(u-r)_{\text{corr}} = u-r-A_{u,Gal}+A_{r,Gal}-K_u(z)+K_r(z). \quad (2)$$

Our final sample consists of 396,718 target galaxies, with median redshift $z_{\text{med}} = 0.107$. We divide our full sample of target galaxies into a blue sequence and a

red sequence using the color divider of James & Ryden (2022):²

$$u - r = 2.391 - 0.1305(M_r + 21.5). \quad (3)$$

With this definition, 184,788 target galaxies lie on the blue side of the divider and 211,930 lie on the red side. Finally, we divided the blue galaxies and the red galaxies into a luminous subsample and a faint subsample at their respective medians: $M_r = -21.163$ for the blue target galaxies, and $M_r = -21.780$ for the red target galaxies. The interquartile range for the blue galaxies is $-21.86 < M_r < -20.32$ and for the red galaxies is $-22.35 < M_r < -21.09$. Figure 1 shows the extinction and K -corrected color-magnitude diagram for our sample of 396,718 target galaxies; the James & Ryden (2022) color divider is plotted as the solid green line.

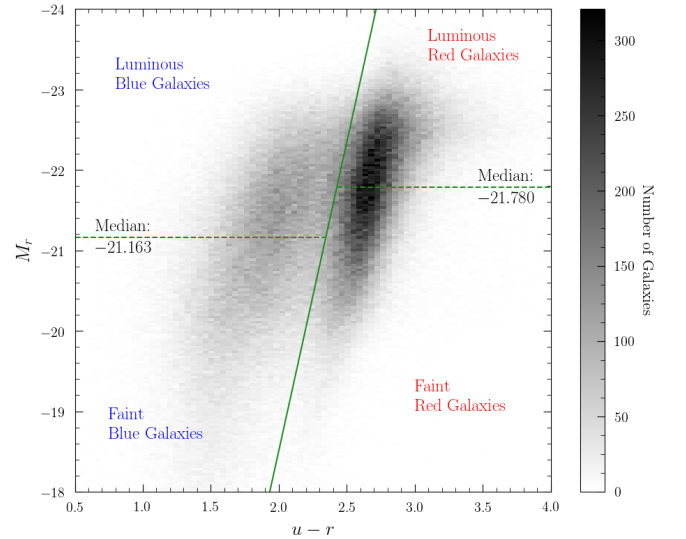


Figure 1. Color-magnitude diagram ($u - r$ versus M_r) for the target galaxies. The four subsamples (luminous blue, luminous red, faint blue, and faint red) are labeled. Solid green line is the color divider of James & Ryden (2022).

For each target galaxy, the position angle ϕ_{pa} is taken from the adaptive moments parameters in the SDSS Legacy database; the phase of the position angle is chosen so that $0^\circ \leq \phi_{\text{pa}} < 180^\circ$, running from north through east. Each target galaxy drawn from the SDSS Legacy spectroscopic survey has associated “surrounding galaxies.” These surrounding galaxies are defined as galaxies from the SDSS Legacy photometric survey

¹ We find that using Petrosian magnitudes (`petroMag`) instead of Model (`modelMag`) and Composite Model magnitudes (`cModelMag`) for color and absolute magnitude does not change the qualitative conclusions of this paper.

² We find that using the color divider of Baldry et al. (2004), based on a shallower sample of SDSS Legacy galaxies, does not change the qualitative conclusions of this paper.

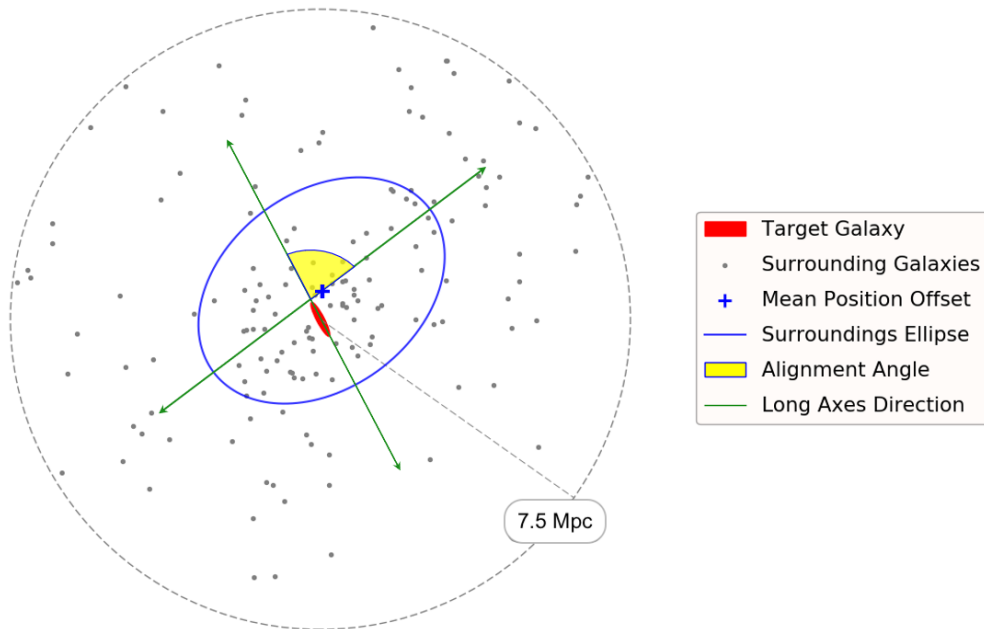


Figure 2. Definition of the alignment angle Φ of the target galaxy (filled red ellipse) relative to the distribution of surrounding galaxies (fitted by the open blue ellipse).

that lie within a projected distance r_p (computed using *astropy*) of the target galaxy, at the target galaxy’s spectroscopic redshift z given the angular separation θ between the target galaxy and the surrounding galaxy. We choose $r_p = 3.0$ Mpc as our primary separation for analyses, but we also consider the broader range of $r_p = 0.1 \rightarrow 7.5$ Mpc. We selected our target galaxies from an area embedded within the main photometric survey footprint, with a buffer of width $\sim 5^\circ$ between the selection area and the survey boundary. This ensures that even for the lowest-redshift target galaxies, none of the surrounding galaxies fall outside the photometric survey footprint.

Since the majority of the surrounding galaxies have photometric data only, they have only photometric redshifts, z_{phot} , rather than the more accurate spectroscopic redshifts of the target galaxies (Beck et al. 2016). To eliminate surrounding galaxies with a high probability of being foreground or background contaminants, we impose the additional constraint that a surrounding galaxy must have $|z - z_{\text{phot}}| < 2\delta z_{\text{phot}}$, where z is the spectroscopic redshift of the target galaxy and δz_{phot} is the rms error in z_{phot} for the surrounding galaxy (Beck et al. 2016). We impose the additional constraint that surrounding galaxies must have $\delta z_{\text{phot}} < 0.04$. Eliminating in this way the galaxies that are likely to be foreground or background galaxies, the median number of surrounding galaxies per target galaxy for a projected separation of $r_p = 3.0$ Mpc ranges from $N_{\text{med}} \approx 500$ for the lowest-redshift target galaxies to $N_{\text{med}} \approx 40$ for

the highest-redshift target galaxies. We also limit our sample to target galaxies with $N \geq 4$ surrounding galaxies, to avoid statistically unreliable alignments; this cut eliminates only 8 target galaxies. For the entire sample of target galaxies, the mean number of surrounding galaxies within a projected distance $r_p = 3.0$ Mpc is $\bar{N} = 177$.

Studies of the alignment of galaxies with surrounding structure have used multiple definitions of the alignment angle Φ (Joachimi et al. 2015); it is thus important to clearly describe our own definition. A target galaxy is at right ascension α_t and declination δ_t . It is surrounded by a population of N surrounding galaxies that survive our cuts in projected separation and photometric redshift. The i^{th} surrounding galaxy has right ascension α_i and declination δ_i . Since the surrounding galaxies are at small angular separation from the target galaxy, we may safely use the “flat celestial sphere” approximation, and compute the coordinates of the surrounding galaxies in a Cartesian system whose origin is at the position of the target galaxy. In this system, the x axis is in the north – south direction, with x increasing northward, while the y axis is in the east – west direction, with y increasing eastward. The position of each surrounding galaxy in this system is

$$x_i = \delta_i - \delta_t, \quad y_i = (\alpha_i - \alpha_t) \cos([\delta_i + \delta_t]/2). \quad (4)$$

Weighing each galaxy equally, the mean offset of the surrounding galaxies from the target galaxy (blue cross

in Figure 2) is given by the first order moments

$$\mu_x = \frac{1}{N} \sum_{i=1}^N x_i, \quad \mu_y = \frac{1}{N} \sum_{i=1}^N y_i. \quad (5)$$

The second order moments are then

$$\begin{aligned} \mu_{xx} &= \frac{1}{N} \sum_{i=1}^N (x_i - \mu_x)^2, & \mu_{yy} &= \frac{1}{N} \sum_{i=1}^N (y_i - \mu_y)^2, \\ \mu_{xy} &= \frac{1}{N} \sum_{i=1}^N (x_i - \mu_x)(y_i - \mu_y). \end{aligned} \quad (6)$$

The shape of the distribution of surrounding galaxies can then be approximated as an ellipse (open blue ellipse in Figure 2) whose position angle ϕ_{sur} is given by the relation

$$\tan(2\phi_{\text{sur}}) = \frac{2\mu_{xy}}{\mu_{xx} - \mu_{yy}} \equiv \beta. \quad (7)$$

With the usual convention that position angle increases from north through east, choosing the correct branch of the tangent function yields the position angle

$$\begin{aligned} \phi_{\text{sur}} &= \frac{1}{2} \tan^{-1} \beta & [\mu_{xx} > \mu_{yy}, \mu_{xy} > 0] \\ \phi_{\text{sur}} &= \frac{1}{2} (180^\circ + \tan^{-1} \beta) & [\mu_{xx} < \mu_{yy}] \\ \phi_{\text{sur}} &= \frac{1}{2} (360^\circ + \tan^{-1} \beta) & [\mu_{xx} > \mu_{yy}, \mu_{xy} < 0]. \end{aligned} \quad (8)$$

Defined in this way, the position angle lies in the range $0^\circ < \phi_{\text{sur}} < 180^\circ$.

Knowing the position angle ϕ_{pa} for the target galaxy and the position angle ϕ_{sur} for the distribution of surrounding galaxies, we define the alignment angle Φ as the angular difference between ϕ_{pa} and ϕ_{sur} , constrained to lie in the interval $0^\circ \leq \Phi \leq 90^\circ$. Figure 2 shows how the alignment angle Φ is defined, using a randomly selected target galaxy as an example.

3. ANALYSIS AND RESULTS

After computing the alignment angle Φ for the target galaxies in our sample, we can examine the distribution of Φ for each of the four subsamples, divided by color and luminosity. Table 1 presents the mean alignment angle and estimated error in the mean for each subsample of target galaxies with surrounding galaxies within $r_p = 3.0 \text{ Mpc}$. If the alignment angle is randomly distributed, we expect a mean alignment angle $\langle \Phi \rangle = 45^\circ$. In Table 1, only the red subsamples show a statistically significant difference from $\langle \Phi \rangle = 45^\circ$. The luminous red (LR) subsample has $\langle \Phi \rangle < 45^\circ$ at the 9.7σ level, while the faint red (FR) subsample also has $\langle \Phi \rangle < 45^\circ$, but at the 4.3σ level. A mean alignment angle slightly less than

Table 1. Alignment Statistics

Galaxy sample	$\langle \Phi \rangle$	# target galaxies
Luminous Blue	$45.140^\circ \pm 0.085^\circ$	92394
Faint Blue	$44.975^\circ \pm 0.085^\circ$	92394
Luminous Red	$44.227^\circ \pm 0.080^\circ$	105965
Faint Red	$44.658^\circ \pm 0.080^\circ$	105965

45° indicates that the images of the red target galaxies have a slight but statistically significant tendency to align parallel to the surrounding structure. On the other hand, the fact that the blue target galaxies have a mean alignment angle indistinguishable from 45° does not necessarily imply that they are randomly oriented relative to the surrounding structure; in a toy model, if half were parallel ($\Phi = 0^\circ$) and half were perpendicular ($\Phi = 90^\circ$) to the surrounding structure, that too would yield $\langle \Phi \rangle = 45^\circ$.

To analyze the results further, we plot a histogram of the distribution of Φ for each subsample, with bins of width $\Delta\Phi = 0.5^\circ$. Figure 3 shows the binned distribution of the normalized alignment angle, $x \equiv \Phi/90^\circ$. To model the distribution function $f(x)$, we assume a linear fit:

$$f(x) = 1 + \eta(x - 0.5). \quad (9)$$

In this normalized linear fit, the only variable parameter is the slope η .

The best fitting slope η and its corresponding 1σ error for each subsample is found by doing a linear least-squares fit; the resulting fits are shown as the red lines in Figure 3. In addition, we perform non-parametric Kolmogorov-Smirnov (KS) tests, comparing the cumulative distribution function for the unbinned data with the cumulative distribution function for our assumed linear fit,

$$F(< x) = x + 0.5\eta(x^2 - x). \quad (10)$$

The gray lines in each panel of Figure 3 represent the range in the slope η for which the KS test yields a probability $P_{\text{ks}} \geq 0.1$. The KS test indicates that both blue subsamples are consistent with having a random distribution of alignment angle: the assumption of $\eta = 0$ yields $P_{\text{ks}} = 0.99$ for the faint blue subsample and $P_{\text{ks}} = 0.41$ for the luminous blue subsample. The red subsamples, however, are strongly inconsistent with having a random distribution of alignment angle: the assumption of $\eta = 0$ yields $P_{\text{ks}} = 5 \times 10^{-4}$ for the faint red subsample and $P_{\text{ks}} = 4 \times 10^{-17}$ for the luminous red subsample.

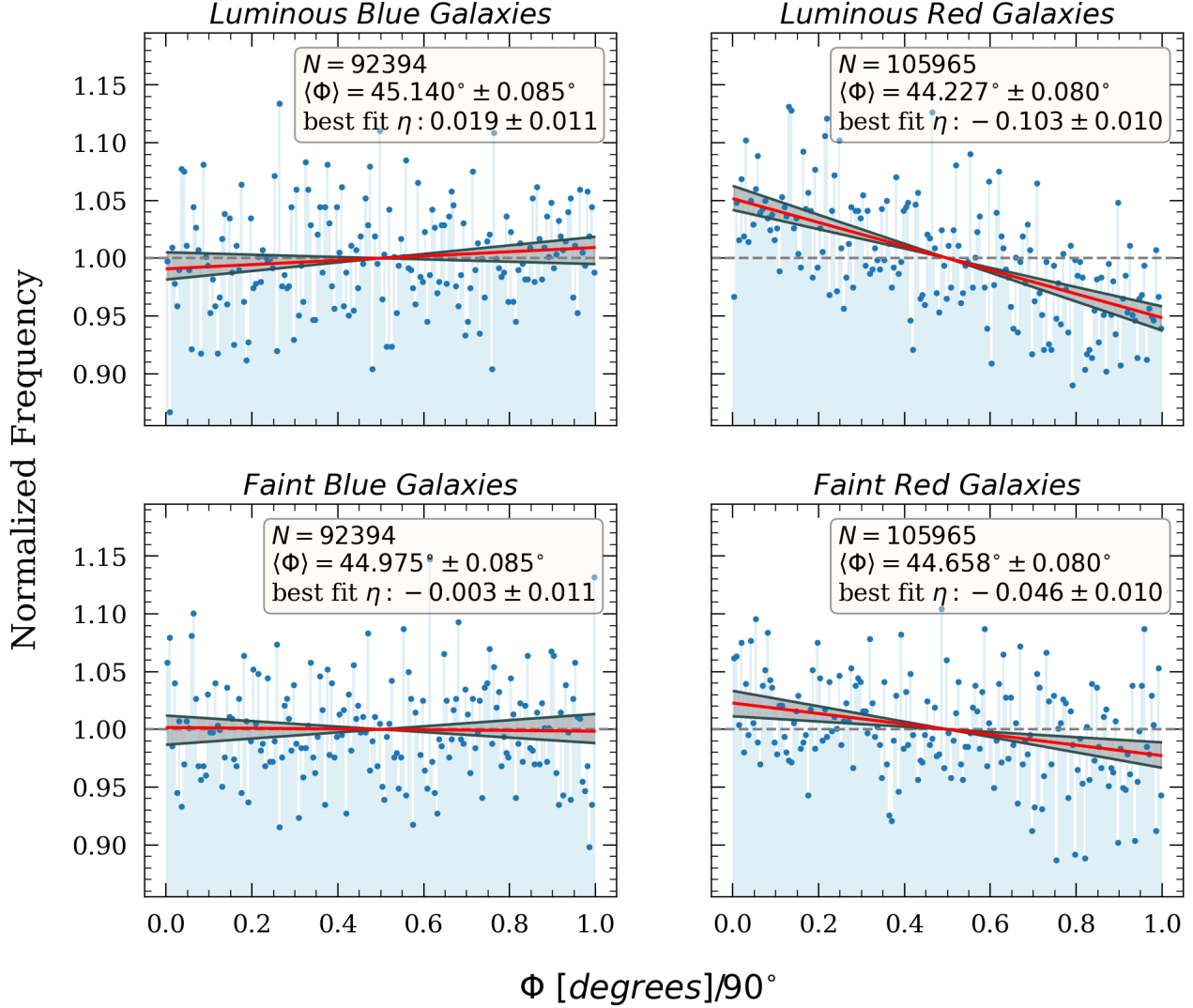


Figure 3. Normalized distribution of alignment angle Φ for the four subsamples of target galaxies. The best linear fit is shown as the red line in each panel. The gray lines indicate the range of slopes that yield $P_{\text{ks}} > 0.1$ in a Kolmogorov-Smirnov test.

The above analysis examines the alignment of galaxy images with the distribution of surrounding galaxies within a projected separation $r_p = 3.0$ Mpc. By varying the limiting projected radius r_p , we can investigate trends in the alignment angle as a function of physical scale. Using the SDSS Legacy Survey, we cannot reliably measure the alignment angle Φ on scales smaller than $r_p \sim 0.1$ Mpc due to an insufficient number of surrounding galaxies per target galaxy, or on scales larger than $r_p \sim 7.5$ Mpc due to the limited survey footprint. Given these limitations, in Figure 4, we plot the average alignment angle when the limiting projected radius lies in the range $r_p = 0.1 \rightarrow 7.5$ Mpc. In Figure 4, the narrowest (yellow) band represents the 1σ error interval, the middle (darker blue) band represents the 3σ error interval, and the broadest (pale blue) band represents

the 5σ error interval. Throughout the entire range of r_p studied, the blue galaxies (left panels in Figure 4) fail to show a significant difference from $\langle\Phi\rangle = 45^\circ$ at a significance level $> 3\sigma$. By contrast, the luminous red galaxies (upper right panel) have $\langle\Phi\rangle < 45^\circ$ at a significance $> 4.5\sigma$ throughout the range of r_p with the average alignment becoming more parallel for smaller r_p . The results for the luminous red galaxies are consistent with $\langle\Phi\rangle \approx 44.5^\circ$ for the outermost bins ($r_p \geq 4$ Mpc). In the range $1 \text{ Mpc} < r_p < 3 \text{ Mpc}$, the mean alignment angle is $\langle\Phi\rangle \approx 44.2^\circ$. At $r_p < 1$ Mpc, the mean alignment angle decreases steadily as r_p becomes smaller, reaching $\langle\Phi\rangle = 42.2^\circ \pm 0.4^\circ$ at $r_p = 0.1$ Mpc.

The range $1 \text{ Mpc} < r_p < 3 \text{ Mpc}$ is also where faint red galaxies (lower right panel of Figure 4) show the most statistically significant alignment (at $> 4.3\sigma$). This

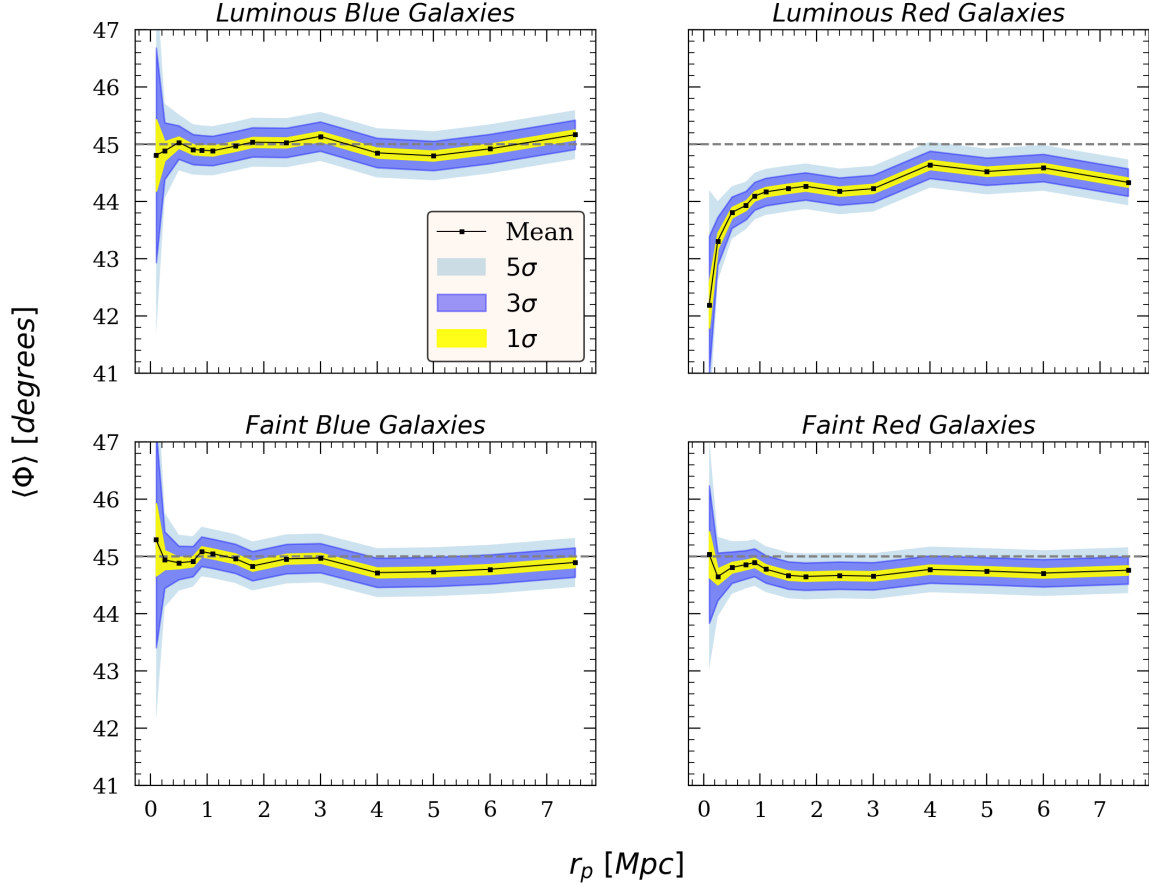


Figure 4. Average alignment angle $\langle\Phi\rangle$ as a function of maximum projected surrounding radius $r_p = 0.1 \rightarrow 7.5$ Mpc for the four subsamples of target galaxies.

range of length scales corresponds to the size of rich clusters of galaxies (Banerjee et al. 2018). On this scale, we are detecting the alignment of bright galaxies with the projected long axis of the cluster as a whole (Tucker & Peterson 1988; Niederste-Ostholt et al. 2010; West et al. 2017). On smaller scales, the luminous red galaxies (which include the brightest cluster galaxies) show a strong parallel alignment with satellite galaxies down to the scale $r_p = 0.1$ Mpc. However, the faint red galaxies in our sample show no statistically significant alignment at $r_p < 1$ Mpc.

To look in more detail at the dependence of alignment angle on luminosity, we plot the average alignment angle as a function of the absolute magnitude for the red and blue samples separately. The data are binned as percentiles, so that each bin contains the same number of target galaxies and there are 100 bins in total. Our large data sample yields 2119 red galaxies per bin, and 1848 blue galaxies per bin. The average alignment angles, binned in this manner, are plotted in Figure 5. The error bars on each point are the standard deviation of the bin divided by the square root of the number in the

bin; that is, the estimated error in the mean. For blue target galaxies, the average alignment angle is consistent with 45° (random orientation) throughout the full range of absolute magnitude. Figure 5(a) shows the average alignment angle versus absolute magnitude within $r_p = 3.0$ Mpc for blue target galaxies; however, the lack of preferred alignment angle holds over the entire range from $r_p = 0.1$ Mpc to $r_p = 7.5$ Mpc. For the red target galaxies, there is a clear trend from a preferred parallel alignment at high luminosities to no preferred alignment at low luminosities. For the most luminous red target galaxies, the tendency for parallel alignment is statistically very strong. This holds for all values of r_p with the average alignment angle following the trend with r_p as shown in Figure 4. Panels (b), (c), and (d) in Figure 5 show the average alignment angle versus absolute magnitudes for the red target galaxies for $r_p = 0.5$, 3.0 , and 7.5 Mpc, respectively. The most luminous 1% of the red target galaxies ($M_r < -23.35$) with surrounding radius $r_p = 3.0$ Mpc, as shown in Figure 5(c), have $\langle\Phi\rangle = 40.49^\circ \pm 0.56^\circ$; this is less than 45° at the 8.1σ level. If we bin together the most luminous 2% of the

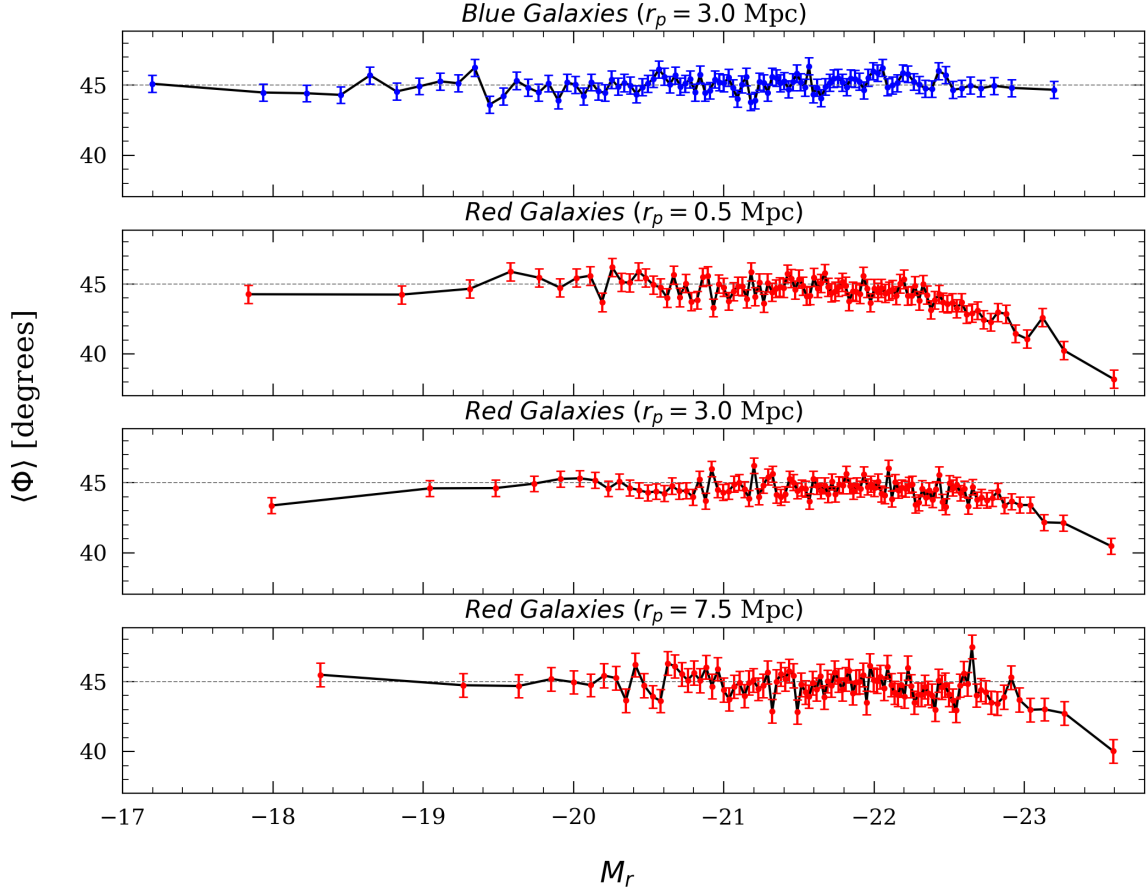


Figure 5. Average alignment angle $\langle\Phi\rangle$ as a function of target galaxy absolute magnitudes M_r for blue and red subsamples, using the color divider of James & Ryden (2022). (a) blue target galaxies with surrounding galaxies out to $r_p = 3.0$ Mpc; (b) red target galaxies with surrounding galaxies out to $r_p = 0.5$ Mpc; (c) red target galaxies with surrounding galaxies out to $r_p = 3.0$ Mpc; (d) red target galaxies with surrounding galaxies out to $r_p = 7.5$ Mpc.

red target galaxies ($M_r < -23.19$), we find that they have $\langle\Phi\rangle = 41.32^\circ \pm 0.40^\circ$ (9.2σ), and the most luminous 3% of the red target galaxies ($M_r < -23.08$) have $\langle\Phi\rangle = 41.60^\circ \pm 0.33^\circ$ (10.3σ).

We performed an additional analysis to determine whether there exists a correlation between the average alignment angle $\langle\Phi\rangle$ and the number N of surrounding galaxies; this indicates whether galaxies in higher-density environments tend to have stronger or weaker alignment signals than those in lower-density environments. We first computed $\bar{N}(z)$, the mean number of surrounding galaxies within a projected distance $r_p = 3.0$ Mpc, as a function of target galaxy redshift. Splitting each sample into lower-density ($N < \bar{N}(z)$) and higher-density ($N > \bar{N}(z)$) subsamples, we computed their average alignment angles. We would see a significant difference between the average alignments of the lower-density and higher-density subsamples if the alignment depends on the local density. The differences between the lower- and higher-density subsam-

ples are consistent with zero for the luminous blue, faint blue, and faint red galaxy subsamples (see the “Local density” columns in Table 2). For the luminous red galaxies, the lower-density ($\langle\Phi_{\text{low}}\rangle = 44.33^\circ \pm 0.11^\circ$) and higher-density ($\langle\Phi_{\text{high}}\rangle = 44.10^\circ \pm 0.12^\circ$) alignment averages are different only at the 1.4σ level.

We also tested to see whether the alignment angle Φ is correlated with the magnitude of a target galaxy’s offset from its surrounding galaxies. For example, a target galaxy at the center of an elongated filament of galaxies may have a different alignment signal from a target galaxy at the end of the filament. The offset of the distribution of surrounding galaxies relative to the target galaxy is given by the first order moments (μ_x, μ_y) in the Cartesian frame centered on the target galaxy (equation 5). This can be converted to a fractional offset f by dividing $(\mu_x^2 + \mu_y^2)^{1/2}$ by the angular equivalent of the projected radius limit $r_p = 3.0$ Mpc. Using their medians ($f_{\text{med,LB}} = 0.10$, $f_{\text{med,FB}} = 0.08$, $f_{\text{med,LR}} = 0.10$, $f_{\text{med,FR}} = 0.09$), we split each of the four subsamples

(LB, FB, LR, and FR) into small offset ($f < f_{\text{med}}$) and large offset ($f > f_{\text{med}}$) samples and computed their average alignment angles. No significant differences were seen for the luminous blue, faint blue, and faint red galaxy samples at $> 0.8\sigma$ level (see the “Fractional offset” columns in Table 2). For the luminous red galaxies, the small offset ($\langle \Phi_{\text{small}} \rangle = 44.12^\circ \pm 0.11^\circ$) and large offset ($\langle \Phi_{\text{large}} \rangle = 44.34^\circ \pm 0.11^\circ$) alignment averages are different at only the 1.4σ level.

When the fractional offset f is non-zero, we can also define a position angle ϕ_{off} of the line segment drawn from the center of the target galaxy, at (0,0) in the Cartesian frame, to the location of the mean position offset at (μ_x, μ_y) . In this way, we can define a new alignment angle Φ_{od} , representing the difference between the position angle ϕ_{pa} of the target galaxy and the position angle ϕ_{off} that points toward the center of the surrounding galaxy distribution. The alignment angle Φ_{od} thus indicates whether a target galaxy at the fringes of an overdense region tends to point toward the center of the overdensity. For all four subsamples of target galaxies (LB, FB, LR, and FR), the mean value $\langle \Phi_{\text{od}} \rangle$ is statistically indistinguishable from 45° , and the distribution of normalized alignment angle ($x \equiv \Phi/90^\circ$) for each subsample is consistent with a random distribution ($\eta = 0$), again verified using the KS test. In addition, we tested for, but did not find, a dependence of $\langle \Phi_{\text{od}} \rangle$ on the magnitude of the fractional offset f .

4. CONCLUSION

The Sloan Digital Sky Survey Legacy survey provides a useful database for looking at the alignment of relatively luminous galaxies with their surrounding large scale structure, as traced out by other galaxies in the survey. In our study, we found that highly luminous red galaxies, with $M_r < -21.78$, have a highly significant tendency for their images to have their long axes align with the long axis of the surrounding structure; this tendency is detectable at a $> 4.5\sigma$ level for a projected length scale $0.1 \text{ Mpc} < r_p \leq 7.5 \text{ Mpc}$. Fainter red galaxies, with $M_r > -21.78$, have a tendency to align in the same sense; however, the alignment signal has significance level $> 4.3\sigma$ in the range $1 \text{ Mpc} < r_p < 3 \text{ Mpc}$. Blue galaxies have no statistically significant tendency for their images to align with the surrounding distribution of galaxies.

The observed difference between alignments of red galaxies and blue galaxies originates in the different physical mechanisms that determine their alignment in space. Red galaxies are generally elliptical galaxies, supported by anisotropic velocity dispersion, rather than being rotationally supported. The linear alignment

model for elliptical galaxies (Catelan et al. 2001) assumes that their shapes are perturbed by an external tidal field produced by the surrounding density distribution. Galaxies close to each other in space experience similar tidal fields and thus have correlated shape distortions (Hirata & Seljak 2004). Since the power spectrum $P(k)$ of cold dark matter density perturbations extends to small wavenumber k , the linear alignment model predicts alignment of elliptical galaxies on large scales ($\sim 10 \text{ Mpc}$ or more), consistent with the results of Okumura et al. (2009), and with our results for red sequence galaxies. By contrast, galaxies at the luminous end of the blue sequence are generally rotationally supported disk galaxies. In the tidal torque model for angular momentum acquisition, galaxy halos are spun up by interaction between their quadrupole moment and the surrounding tidal field. However, although the tidal torque model predicts an alignment between the spin axis of a halo and its surrounding density field, the spin axis of the stellar disk is often misaligned with that of the halo it inhabits, as a result of merging subhalos and accretion events (Cen 2014; Chisari et al. 2017; Lee et al. 2018). Thus, a lack of alignment for disk galaxies with surrounding structure is not surprising, even on scales $\sim 1 \text{ Mpc}$.

Our method for quantifying alignment between galaxy images and larger scale structure was useful over projected length scales from $r_p \sim 0.1 \text{ Mpc}$ to $r_p \sim 7.5 \text{ Mpc}$ using data from the SDSS Legacy survey. Over this range of scales, running from the size of an individual galaxy and its satellites to the correlation length for the distribution of galaxy clusters, a knowledge of intrinsic alignments is important for understanding the interplay between galaxy evolution and the evolution of large scale structure in the universe. The same technique that we used to measure alignment angles in this work can be applied to projections of 3-dimensional numerical simulations, giving further insight into the evolution of alignment with decreasing redshift, and the dependence of alignment on the non-gravitational physics involved in the formation and evolution of galaxies.

5. ACKNOWLEDGEMENTS

This project was begun during the Summer Undergraduate Research Program of the Ohio State University Department of Astronomy, with support from the Center for Cosmology and AstroParticle Physics (CCAPP). We thank Derrick James of the Ohio State University School of Earth Sciences for his assistance with the color dividers.

Funding for the Sloan Digital Sky Survey IV has been provided by the Alfred P. Sloan Foundation, the U.S.

Table 2. Average Alignment Angle $\langle\Phi\rangle$ vs Local Density and Fractional Offset

Galaxy sample	Local Density		Fractional Offset	
	Lower density ($N < \bar{N}(z)$)	Higher density ($N > \bar{N}(z)$)	Small offset ($f < f_{med}$)	Large offset ($f > f_{med}$)
Luminous Blue	$45.14^\circ \pm 0.11^\circ$	$45.14^\circ \pm 0.14^\circ$	$45.16^\circ \pm 0.12^\circ$	$45.12^\circ \pm 0.12^\circ$
Faint Blue	$44.98^\circ \pm 0.11^\circ$	$44.98^\circ \pm 0.14^\circ$	$44.95^\circ \pm 0.12^\circ$	$45.00^\circ \pm 0.12^\circ$
Luminous Red	$44.33^\circ \pm 0.11^\circ$	$44.10^\circ \pm 0.12^\circ$	$44.12^\circ \pm 0.11^\circ$	$44.34^\circ \pm 0.11^\circ$
Faint Red	$44.67^\circ \pm 0.11^\circ$	$44.64^\circ \pm 0.12^\circ$	$44.72^\circ \pm 0.11^\circ$	$44.60^\circ \pm 0.11^\circ$

Department of Energy Office of Science, and the Participating Institutions. SDSS-IV acknowledges support and resources from the Center for High Performance Computing at the University of Utah. The SDSS website is www.sdss.org.

SDSS-IV is managed by the Astrophysical Research Consortium for the Participating Institutions of the SDSS Collaboration including the Brazilian Participation Group, the Carnegie Institution for Science, Carnegie Mellon University, Center for Astrophysics — Harvard & Smithsonian, the Chilean Participation Group, the French Participation Group, Instituto de Astrofísica de Canarias, The Johns Hopkins University, Kavli Institute for the Physics and Mathematics of the Universe (IPMU) / University of Tokyo, the Korean Participation Group, Lawrence Berkeley National

Laboratory, Leibniz Institut für Astrophysik Potsdam (AIP), Max-Planck-Institut für Astronomie (MPIA Heidelberg), Max-Planck-Institut für Astrophysik (MPA Garching), Max-Planck-Institut für Extraterrestrische Physik (MPE), National Astronomical Observatories of China, New Mexico State University, New York University, University of Notre Dame, Observatório Nacional / MCTI, The Ohio State University, Pennsylvania State University, Shanghai Astronomical Observatory, United Kingdom Participation Group, Universidad Nacional Autónoma de México, University of Arizona, University of Colorado Boulder, University of Oxford, University of Portsmouth, University of Utah, University of Virginia, University of Washington, University of Wisconsin, Vanderbilt University, and Yale University.

REFERENCES

- Ahumada, R., Prieto, C. A., Almeida, A., et al. 2020, ApJS, 249, 3, doi: [10.3847/1538-4365/ab929e](https://doi.org/10.3847/1538-4365/ab929e)
- Astropy Collaboration, Robitaille, T. P., Tollerud, E. J., et al. 2013, A&A, 558, A33, doi: [10.1051/0004-6361/201322068](https://doi.org/10.1051/0004-6361/201322068)
- Astropy Collaboration, Price-Whelan, A. M., Sipőcz, B. M., et al. 2018, AJ, 156, 123, doi: [10.3847/1538-3881/aabc4f](https://doi.org/10.3847/1538-3881/aabc4f)
- Baldry, I. K., Glazebrook, K., Brinkmann, J., et al. 2004, ApJ, 600, 681, doi: [10.1086/380092](https://doi.org/10.1086/380092)
- Banerjee, P., Szabo, T., Pierpaoli, E., et al. 2018, NewA, 58, 61, doi: [10.1016/j.newast.2017.07.008](https://doi.org/10.1016/j.newast.2017.07.008)
- Beck, R., Dobos, L., Budavári, T., Szalay, A. S., & Csabai, I. 2016, MNRAS, 460, 1371, doi: [10.1093/mnras/stw1009](https://doi.org/10.1093/mnras/stw1009)
- Bhowmick, A. K., Chen, Y., Tenneti, A., Di Matteo, T., & Mandelbaum, R. 2020, MNRAS, 491, 4116, doi: [10.1093/mnras/stz3240](https://doi.org/10.1093/mnras/stz3240)
- Blanton, M. R., & Roweis, S. 2007, AJ, 133, 734, doi: [10.1086/510127](https://doi.org/10.1086/510127)
- Blazek, J., Vlah, Z., & Seljak, U. 2015, JCAP, 2015, 015, doi: [10.1088/1475-7516/2015/08/015](https://doi.org/10.1088/1475-7516/2015/08/015)
- Bridle, S., & King, L. 2007, New Journal of Physics, 9, 444, doi: [10.1088/1367-2630/9/12/444](https://doi.org/10.1088/1367-2630/9/12/444)
- Brown, F. G. 1939, MNRAS, 99, 534, doi: [10.1093/mnras/99.6.534](https://doi.org/10.1093/mnras/99.6.534)
- . 1964, MNRAS, 127, 517, doi: [10.1093/mnras/127.6.517](https://doi.org/10.1093/mnras/127.6.517)
- Catelan, P., Kamionkowski, M., & Blandford, R. D. 2001, MNRAS, 320, L7, doi: [10.1046/j.1365-8711.2001.04105.x](https://doi.org/10.1046/j.1365-8711.2001.04105.x)
- Cen, R. 2014, ApJL, 785, L15, doi: [10.1088/2041-8205/785/1/L15](https://doi.org/10.1088/2041-8205/785/1/L15)
- Chen, Y.-C., Ho, S., Blazek, J., et al. 2019, MNRAS, 485, 2492, doi: [10.1093/mnras/stz539](https://doi.org/10.1093/mnras/stz539)
- Chisari, N. E., Koukoufilippas, N., Jindal, A., et al. 2017, MNRAS, 472, 1163, doi: [10.1093/mnras/stx1998](https://doi.org/10.1093/mnras/stx1998)
- Codis, S., Jindal, A., Chisari, N. E., et al. 2018, MNRAS, 481, 4753, doi: [10.1093/mnras/sty2567](https://doi.org/10.1093/mnras/sty2567)
- Doi, M., Tanaka, M., Fukugita, M., et al. 2010, AJ, 139, 1628, doi: [10.1088/0004-6256/139/4/1628](https://doi.org/10.1088/0004-6256/139/4/1628)
- Ebrahimi, E., & Abolhasani, A. 2022, ApJ, 926, 200, doi: [10.3847/1538-4357/ac497c](https://doi.org/10.3847/1538-4357/ac497c)

- Eisenstein, D. J., Annis, J., Gunn, J. E., et al. 2001, *AJ*, 122, 2267, doi: [10.1086/323717](https://doi.org/10.1086/323717)
- Eisenstein, D. J., Weinberg, D. H., Agol, E., et al. 2011, *AJ*, 142, 72, doi: [10.1088/0004-6256/142/3/72](https://doi.org/10.1088/0004-6256/142/3/72)
- Fortuna, M. C., Hoekstra, H., Johnston, H., et al. 2021, *A&A*, 654, A76, doi: [10.1051/0004-6361/202140706](https://doi.org/10.1051/0004-6361/202140706)
- Fukugita, M., Ichikawa, T., Gunn, J. E., et al. 1996, *AJ*, 111, 1748, doi: [10.1086/117915](https://doi.org/10.1086/117915)
- Ganeshaiah Veena, P., Cautun, M., Tempel, E., van de Weygaert, R., & Frenk, C. S. 2019, *MNRAS*, 487, 1607, doi: [10.1093/mnras/stz1343](https://doi.org/10.1093/mnras/stz1343)
- Georgiou, C., Chisari, N. E., Fortuna, M. C., et al. 2019a, *A&A*, 628, A31, doi: [10.1051/0004-6361/201935810](https://doi.org/10.1051/0004-6361/201935810)
- Georgiou, C., Johnston, H., Hoekstra, H., et al. 2019b, *A&A*, 622, A90, doi: [10.1051/0004-6361/201834219](https://doi.org/10.1051/0004-6361/201834219)
- Ghosh, B., Durrer, R., & Schäfer, B. M. 2021, *MNRAS*, 505, 2594, doi: [10.1093/mnras/stab1435](https://doi.org/10.1093/mnras/stab1435)
- Gunn, J. E. 1967, *ApJ*, 150, 737, doi: [10.1086/149378](https://doi.org/10.1086/149378)
- Gunn, J. E., Siegmund, W. A., Mannery, E. J., et al. 2006, *AJ*, 131, 2332, doi: [10.1086/500975](https://doi.org/10.1086/500975)
- Hilbert, S., Xu, D., Schneider, P., et al. 2017, *MNRAS*, 468, 790, doi: [10.1093/mnras/stx482](https://doi.org/10.1093/mnras/stx482)
- Hirata, C. M., Mandelbaum, R., Ishak, M., et al. 2007, *MNRAS*, 381, 1197, doi: [10.1111/j.1365-2966.2007.12312.x](https://doi.org/10.1111/j.1365-2966.2007.12312.x)
- Hirata, C. M., & Seljak, U. 2004, *PhRvD*, 70, 063526, doi: [10.1103/PhysRevD.70.063526](https://doi.org/10.1103/PhysRevD.70.063526)
- Hirv, A., Pelt, J., Saar, E., et al. 2017, *A&A*, 599, A31, doi: [10.1051/0004-6361/201629248](https://doi.org/10.1051/0004-6361/201629248)
- Hogg, D. W., Baldry, I. K., Blanton, M. R., & Eisenstein, D. J. 2002, arXiv e-prints, astro. <https://arxiv.org/abs/astro-ph/0210394>
- Hoyle, F. 1951, in *Problems of Cosmical Aerodynamics*, 195
- James, D., & Ryden, B. S. 2022, *Research Notes of the AAS*, 6, 108, doi: [10.3847/2515-5172/ac73f1](https://doi.org/10.3847/2515-5172/ac73f1)
- Joachimi, B., Cacciato, M., Kitching, T. D., et al. 2015, *SSRv*, 193, 1, doi: [10.1007/s11214-015-0177-4](https://doi.org/10.1007/s11214-015-0177-4)
- Johnston, H., Georgiou, C., Joachimi, B., et al. 2019, *A&A*, 624, A30, doi: [10.1051/0004-6361/201834714](https://doi.org/10.1051/0004-6361/201834714)
- Jones, B. J. T., van de Weygaert, R., & Aragón-Calvo, M. A. 2010, *MNRAS*, 408, 897, doi: [10.1111/j.1365-2966.2010.17202.x](https://doi.org/10.1111/j.1365-2966.2010.17202.x)
- Kraljic, K., Duckworth, C., Tojeiro, R., et al. 2021, *MNRAS*, 504, 4626, doi: [10.1093/mnras/stab1109](https://doi.org/10.1093/mnras/stab1109)
- Lee, J., & Pen, U.-L. 2007, *ApJL*, 670, L1, doi: [10.1086/524032](https://doi.org/10.1086/524032)
- Lee, J., Kim, S., Jeong, H., et al. 2018, *ApJ*, 864, 69, doi: [10.3847/1538-4357/aad54e](https://doi.org/10.3847/1538-4357/aad54e)
- Niederste-Ostholt, M., Strauss, M. A., Dong, F., Koester, B. P., & McKay, T. A. 2010, *MNRAS*, 405, 2023, doi: [10.1111/j.1365-2966.2010.16597.x](https://doi.org/10.1111/j.1365-2966.2010.16597.x)
- Okumura, T., & Jing, Y. P. 2009, *ApJL*, 694, L83, doi: [10.1088/0004-637X/694/1/L83](https://doi.org/10.1088/0004-637X/694/1/L83)
- Okumura, T., Jing, Y. P., & Li, C. 2009, *ApJ*, 694, 214, doi: [10.1088/0004-637X/694/1/214](https://doi.org/10.1088/0004-637X/694/1/214)
- Paz, D. J., Stasyszyn, F., & Padilla, N. D. 2008, *MNRAS*, 389, 1127, doi: [10.1111/j.1365-2966.2008.13655.x](https://doi.org/10.1111/j.1365-2966.2008.13655.x)
- Pedersen, E. M., Yao, J., Ishak, M., & Zhang, P. 2020, *ApJL*, 899, L5, doi: [10.3847/2041-8213/aba51b](https://doi.org/10.3847/2041-8213/aba51b)
- Peebles, P. J. E. 1969, *ApJ*, 155, 393, doi: [10.1086/149876](https://doi.org/10.1086/149876)
- Planck Collaboration, Aghanim, N., Akrami, Y., et al. 2020, *A&A*, 641, A6, doi: [10.1051/0004-6361/201833910](https://doi.org/10.1051/0004-6361/201833910)
- Reaves, G. 1958, *PASP*, 70, 461, doi: [10.1086/127270](https://doi.org/10.1086/127270)
- Reischke, R., & Schäfer, B. M. 2019, *JCAP*, 2019, 031, doi: [10.1088/1475-7516/2019/04/031](https://doi.org/10.1088/1475-7516/2019/04/031)
- Rodriguez, F., Merchán, M., & Artale, M. C. 2022, arXiv e-prints, arXiv:2204.00683. <https://arxiv.org/abs/2204.00683>
- Samuroff, S., Mandelbaum, R., & Blazek, J. 2020, arXiv e-prints, arXiv:2009.10735. <https://arxiv.org/abs/2009.10735>
- Sanders, J. L., & Evans, N. W. 2017, *MNRAS*, 472, 2670, doi: [10.1093/mnras/stx2116](https://doi.org/10.1093/mnras/stx2116)
- Schlafly, E. F., & Finkbeiner, D. P. 2011, *ApJ*, 737, 103, doi: [10.1088/0004-637X/737/2/103](https://doi.org/10.1088/0004-637X/737/2/103)
- Schlegel, D. J., Finkbeiner, D. P., & Davis, M. 1998, *ApJ*, 500, 525, doi: [10.1086/305772](https://doi.org/10.1086/305772)
- Scranton, R., Connolly, A. J., Szalay, A. S., et al. 2005, arXiv e-prints, astro. <https://arxiv.org/abs/astro-ph/0508564>
- Smargon, A., Mandelbaum, R., Bahcall, N., & Niederste-Ostholt, M. 2012, *MNRAS*, 423, 856, doi: [10.1111/j.1365-2966.2012.20923.x](https://doi.org/10.1111/j.1365-2966.2012.20923.x)
- Strauss, M. A., Weinberg, D. H., Lupton, R. H., et al. 2002, *AJ*, 124, 1810, doi: [10.1086/342343](https://doi.org/10.1086/342343)
- Tenneti, A., Kitching, T. D., Joachimi, B., & Di Matteo, T. 2021, *MNRAS*, 501, 5859, doi: [10.1093/mnras/staa3934](https://doi.org/10.1093/mnras/staa3934)
- Tonegawa, M., & Okumura, T. 2022, *ApJL*, 924, L3, doi: [10.3847/2041-8213/ac4246](https://doi.org/10.3847/2041-8213/ac4246)
- Tucker, G. S., & Peterson, J. B. 1988, *AJ*, 95, 298, doi: [10.1086/114637](https://doi.org/10.1086/114637)
- Wang, P., Guo, Q., Libeskind, N. I., et al. 2019, *MNRAS*, 484, 4325, doi: [10.1093/mnras/stz285](https://doi.org/10.1093/mnras/stz285)
- Wang, P., Libeskind, N. I., Tempel, E., et al. 2020, *ApJ*, 900, 129, doi: [10.3847/1538-4357/aba6ea](https://doi.org/10.3847/1538-4357/aba6ea)
- Wang, P., Luo, Y., Kang, X., et al. 2018, *ApJ*, 859, 115, doi: [10.3847/1538-4357/aabe2b](https://doi.org/10.3847/1538-4357/aabe2b)

- Wang, Y., Yang, X., Mo, H. J., et al. 2008, MNRAS, 385, 1511, doi: [10.1111/j.1365-2966.2008.12927.x](https://doi.org/10.1111/j.1365-2966.2008.12927.x)
- West, M. J., de Propriis, R., Bremer, M. N., & Phillipps, S. 2017, Nature Astronomy, 1, 0157, doi: [10.1038/s41550-017-0157](https://doi.org/10.1038/s41550-017-0157)
- Wyatt, S. P., J., & Brown, F. G. 1955, AJ, 60, 415, doi: [10.1086/107250](https://doi.org/10.1086/107250)
- York, D. G., Adelman, J., Anderson, John E., J., et al. 2000, AJ, 120, 1579, doi: [10.1086/301513](https://doi.org/10.1086/301513)
- Zhang, Y., Yang, X., & Guo, H. 2020, MNRAS, 500, 1895, doi: [10.1093/mnras/staa2356](https://doi.org/10.1093/mnras/staa2356)
- Zhang, Y., Yang, X., Wang, H., et al. 2015, ApJ, 798, 17, doi: [10.1088/0004-637X/798/1/17](https://doi.org/10.1088/0004-637X/798/1/17)
- . 2013, ApJ, 779, 160, doi: [10.1088/0004-637X/779/2/160](https://doi.org/10.1088/0004-637X/779/2/160)
- Zjupa, J., Schäfer, B. M., & Hahn, O. 2020, arXiv e-prints, arXiv:2010.07951. <https://arxiv.org/abs/2010.07951>